SUPPLEMENTARY INFORMATION

"Cardiac troponin T N-domain variant destabilizes the actin interface resulting in disturbed myofilament function."

Maicon Landim-Vieira[1], Weikang Ma[2], Taejeong Song[3], Hosna Rastegarpouyani[4,5], Henry Gong[2], Isabella Leite Coscarella[1], Sylvia Bogaards[6], Stefan Conijn[6], Coen Ottenheijm[6], Hyun Seok Hwang[7], Maria Papadaki[8], Bjorn Knollmann[9], Sakthivel Sadayappan[3], Thomas Irving[2], Vitold Galkin[10], P. Bryant Chase[4], J. Renato Pinto[1]

Corresponding author: Jose R. Pinto

Email: jose.pinto@med.fsu.edu

This PDF file includes:

Supplementary text

Supplemental Figures 1 to 9

Supplemental Tables 1 to 5

SI References

Supplementary Information Text

SI Materials and Methods.

Ca^{2+} solutions

Ca^{2+} solutions were calculated utilizing the pCa Calculator (1) and contained: 20mM 3-[N-morpholino] propanesulfonic acid (MOPS), 7mM ethylene glycol-bis(2-aminoethylether)-N,N,N′,N′-tetra acetic acid (EGTA), 15mM phosphocreatine, 15 units mL^{-1} creatine phosphokinase, 2.5mM $MgATP^{2-}$, 1mM free Mg^{2+}, ionic strength maintained constant at 150mM by adding Kpropionate, varying [Ca^{2+}], pH 7.0. The anion of choice for the pCa solutions was propionate (e.g., $CaPr_2$, $MgPr_2$ and KPr). All solutions were made, and experiments were performed at room temperature (20–21°C).

Cardiac muscle preparations

Permeabilized cardiac muscles were prepared as previously described (2, 3). Excised NTg and Tg-I79N hearts were cut-open along the septum to expose the left ventricle to 1% Triton X-100 (v:v) in a pCa 8 relaxing solution (150mM ionic strength, 2.5mM $MgATP^{2-}$, pH 7). Cardiac muscles were incubated for 4 h in Triton X-100 permeabilizing solution at 4°C. Later, the solution was changed to a relaxing pCa 8 solution containing 51% glycerol (v:v) and stored at −20°C. For muscle mechanics, permeabilized left ventricular papillary muscles were isolated and dissected, their ends attached to aluminum T-clips, and end compliance was minimized by chemically fixing the tissue ends using 1% glutaraldehyde (4). Sarcomere length (SL) was set to either 2.1 μm and 2.3 μm at pCa 8 using HeNe laser diffraction.

Muscle mechanics

Force levels were measured by a force transducer (Aurora Scientific Inc. Model 403A) while muscle length was controlled by a high-speed servomotor (Aurora Scientific Inc. Model 322C). The Ca^{2+}-dependence of steady-state, isometric force was obtained after exposing the cardiac muscle to a series of Ca^{2+} solutions ranging from pCa 8.0 to 4.0 at 21 °C. pCa_{50} and n_{Hill} were estimated by fitting the data using a 2-parameter Hill equation as described (5). pCa-force plots (Fig. 2 A-B) were fit using a 3-parameter Hill equation (5). After force reached steady-state in each pCa solution, muscle mechanics were measured as previously described (2, 3). Kinetics of tension redevelopment (k_{TR}) was obtained by rapidly shortening

the cardiac muscle by 19% of its initial length (L_0) for 20 ms followed by rapid re-stretch (25% L_0). Then, the cardiac muscle preparation was returned back to L_0. The apparent rate constant *k* was obtained from each tension recovery time course as previously described (2). Sinusoidal stiffness (SS) measurements were recorded as previously described (2). Briefly, cardiac muscle was oscillated in 0.2% L_0 (peak-to-peak) at 100 Hz with a sampling rate of 1 kHz. All SS data were analyzed using R Studio and fit with a 4-parameter Hill equation (3).

Mathematical modeling

Estimations of attachment rate (*f*), detachment rate (*g*), and k_{OFF} were obtained by modeling the relationship between isometric steady-state force and k_{TR} using the 3-state model of muscle contraction in MatLab as previously described (2). k_{ON} was held constant according to measurements obtained experimentally using wild type or HCM-containing thin filaments in the presence of myosin and MgATP (2, 6).

Western immunoblotting

NTg and Tg-I79N left ventricular myocardium was lysed in RIPA buffer containing 1:100 protease and phosphatase inhibitors (Sigma; Cat. No. P1860 and P0044, respectively). Protein concentrations were then measured using a BCA protein assay kit (Pierce, Cat. No. 23225). 15 µg of protein from each of the samples were subjected to electrophoresis in 12% SDS-PAGE gel at 100 V. Next, the proteins were transferred to nitrocellulose membranes using the iBlot™ 2 dry blotting system at 20 V for 7 min at room temperature. The membranes were blocked with iBind™ flex FD solution for 30 min at room temperature with gentle agitation. Next, the membranes were placed in the iBind™ flex western device and probed with primary antibodies: rabbit polyclonal anti-GAPDH (Santa Cruz (F L-335): sc-25778) at 1:1000 dilution; mouse monoclonal anti-β-tubulin (E7, Developmental Studies Hybridoma Bank, University of Iowa) at 1:400 dilution; rabbit polyclonal anti-MYBPC3-P_{ser282} (custom-made, gift from Dr. Sakthivel Sadayappan, University of Cincinnati) at 1:2000 dilution; mouse monoclonal anti-MYBPC3 (Santa Cruz (E-7): sc-137180) at 1:400 dilution; rabbit polyclonal anti-cTnI-$P_{ser23/24}$ (Cell Signaling; Cat #4004) at 1:200 dilution; mouse monoclonal anti-cTnI total (TI-1, Developmental Studies Hybridoma Bank, University of Iowa) at 1:400 dilution; mouse monoclonal anti-α-tubulin (12G10, Developmental Studies Hybridoma Bank, University of Iowa) at 1:400 dilution; mouse monoclonal anti-α-tubulin acetylated (Sigma Aldrich, T7451) at 1:200

dilution, and rabbit monoclonal anti-α-tubulin detyrosinated (RevMAb Biosciences, clone RM444) at 1:200 dilution. The secondary antibodies were donkey anti-rabbit (IRDye 800CW; LI-COR™) at 1:1000 dilution, goat anti-rabbit (IRDye 680RD; LI-COR™) at 1:1000 dilution, goat anti-mouse (IRDye 800CW; LI-COR™) at 1:1000 dilution, and donkey anti-mouse (IRDye 680LT; LI-COR™) at 1:1000 dilution. Both primary and secondary antibodies were prepared in iBind™ flex FD solution. The membranes were washed three times (5 min each) with TBS with 0.05% Tween™ 20. Lastly, the membranes were imaged using the Odyssey™ CLx imaging system (LI-COR™) and quantified using the ImageStudio version 4 (LI-COR™).

Phos-tag followed by immunoblotting: NTg and Tg-I79N left ventricular myocardium was lysed in RIPA buffer containing 1:100 protease and phosphatase inhibitors (Sigma; Cat. No. P1860 and P0044, respectively). Protein concentrations were then measured using a BCA protein assay kit (Pierce, Cat. No. 23225). 3 µg of protein from each of the samples were subjected to electrophoresis in 12% SDS-PAGE gel with 20 µM Phos-tag™ Acrylamide (FUJIFILM Wako Chemicals) and 100 µM manganese chloride at 90 V at room temperature. The proteins were transferred to a nitrocellulose membrane using the iBlot™ 2 dry blotting system at 20 V for 7 min at room temperature. The membrane was blocked with iBind™ flex FD solution for 30 min at room temperature with gentle agitation. Next, the membrane was placed in the iBind™ flex western device and incubated with mouse monoclonal anti-myosin light chain primary antibody (Enzo, F109.3E1) at 1:10 dilution and donkey anti-mouse (IRDye 680RD, LI-COR™) at 1:1000 dilution. Both antibodies were prepared in iBind™ flex FD solution. Membrane was washed three times (5 min each) with PBS with 0.05% Tween™ 20. Lastly, the membrane was imaged using the Odyssey™ CLx imaging system (LI-COR™) and ImageStudio™ (LI-COR™) was used for band intensity quantification. RLC phosphorylation ratio was quantified by dividing the intensity of the RLC-P (top band) over the sum of both non-phosphorylated plus phosphorylated intensities.

Cardiac thin filament length

Left ventricular papillary muscles were dissected into small bundles, slightly stretched, permeabilized, and fixed in 4% PF (Sigma #F1635) in PBS for 10 min at room temperature. To stain the cardiac thin filaments, the samples were incubated for two days with 1:20 Alexa Fluor 488–conjugated Phalloidin (Invitrogen #A12379) in PBS. Samples were then washed and mounted in Mowiol. Z-stacks images were made on a Leica TCS SP8 STED 3X (Leica Microsystems) using an oil immersion objective HCX

PL APO STD ×100 (numerical aperture 1.4) and gated Hybrid Detectors. Images were deconvolved using Huygens Professional (SVI) software. Line scans were made along the long axis of the cardiomyocytes using ImageJ software, and intensity plot profiles were generated. Using Fityk software, the profiles were fit with a Gaussian function to determine thin filament length as previously described (7). Sarcomere length was determined from the Gaussian fits.

Small-angle X-ray diffraction

Mouse myocardium preparations – All procedures using live mice were done in accordance with protocols approved by the Institutional Animal Care and Use Committees (IACUCs) of the Florida State University and the Illinois Institute of Technology. Mice were euthanized by deep anesthesia with isoflurane followed by cervical dislocation. Left ventricle papillary muscles were dissected from mice and permeabilized with 1% Triton X-100 in relaxing solution (containing in mM: 6.3 Na2ATP, 6.48 MgCl2, 10 EGTA, 100 BES, 10 phosphocreatine, 49.76 KPropionate, 10 DTT, and creatine kinase 10 U/ml) overnight. The muscles were washed with fresh cold relaxing solution and muscles were further dissected into fiber strips, clipped on aluminum T-clips and stored in cold relaxing solution for the day's experiments.

Small-angle X-diffraction – Equatorial X-ray diffraction patterns were collected from freshly permeabilized muscle strips using the small-angle instrument on the BioCAT beamline 18ID at the Advanced Photon Source, Argonne National Laboratory (8). The X-ray beam was focused to ~0.06 × 0.15 mm at the detector plane. The sample-to-detector distance was ~3.5 m and the X-ray wavelength was 0.103 nm. Clipped tissue bundles (~200 µm diameter, 2-3 mm long) were mounted between a force transducer (Model 402A, Aurora Scientific) and a static hook. Force was monitored using Muscle Dynamic Control system (Model 610A, Aurora Scientific). Sarcomere length was adjusted by laser diffraction using a 4-mW HeNe laser. Diffraction patterns were collected at sarcomere lengths of 2.1 µm and 2.3 µm. X-ray exposures were 1 s at an incident flux of $\sim 3\times10^{12}$ photons per second, and the patterns were collected on a CCD-based X-ray detector (Mar 165; Rayonix Inc. Evanston, IL).

X-ray data analysis – The data were analyzed using data reduction programs from the MuscleX software package developed at BioCAT (9). The spacings and intensities of the 1,0 and 1,1 equatorial reflections were measured by the "Equator" routine in MuscleX as described previously (10). The angular divergence of the 1,0 equatorial X-ray reflections was measured by the "Scanning Diffraction" routine in the MuscleX

software package as described previously (11). Intensity (I_{M3}) of the third myosin meridional reflection (M3) was measured using the "Projection Traces" routine in MuscleX as described previously (12).

Electron Microscopy:

NTg and Tg-I79N mice were euthanized by cervical dislocation. Hearts were dissected out, and quickly perfused first with 0.1M cacodylate buffer followed by Karnovsky's fixative (3% paraformaldehyde, 2.5% glutaraldehyde in 0.2M sodium cacodylate buffer, pH 7.4). The samples were then sliced longitudinally into two halves each containing right and left ventricles. Left ventricular papillary muscles were hand sectioned into 1x1x3 mm longitudinal blocks, and kept in fixative at 4°C overnight. Secondary fixation was carried out using 1% OsO_4 with 1.5% KFe for 30 minutes then 1% OsO_4 for 60 minutes. Overnight staining with %1 uranyl acetate was followed by series of ethanol and propylene oxide dehydrations. Tissues were embedded in Epoxy resin embedding medium (25 mL embed-812, 15 mL araldite 502, 55 mL DDSA, 1.75 mL DMP-30) and kept in an oven at 60°C for 48 hours. Ultrathin sections (40 nm) were collected and placed on 200-mesh copper grids. Electron micrographs at 12x, 20x, and 40x magnification were recorded using Hitachi electron microscope (HT7800) operated at 100 kV. Best quality images with distinct sarcomeric bands (A-band, I-band, M-band, and Z-line) were selected for data analysis. ImageJ 1.53a was used to measure the length of the sarcomeres, length of the sarcomeric bands, and the thickness of the Z-line.

SRX/DRX measurements

The skinning methods used in these experiments were as previously described (13, 14). Briefly, papillary muscles from the left ventricle were skinned on ice for 6 hours in a buffer consisting of (in mM) 100 NaCl, 8 $MgCl_2$, 5 EGTA, 5 K_2HPO_4, 5 KH_2PO_4, 3 NaN_3, 5 ATP, 1 DTT, 20 BDM and 0.1% (v/v) Triton X-100 at pH 7. The solution was refreshed every two hours. The permeabilized papillary muscles were incubated overnight at 4°C in a glycerinating buffer (in mM): 120 K acetate, 5 Mg acetate, 5 EGTA, 2.5 K_2HPO_4, 2.5 KH_2PO_4, 50 MOPS, 5 ATP, 20 BDM, 2 DTT, and 50% (v/v) glycerol at pH 6.8. Next day, samples were stored in fresh glycerinating solution at -20°C until use.

On the day of experiment, permeabilized left ventricular papillary muscle was dissected into a small bundle of fibers in cold glycerol buffer. As previously described, each bundle was placed in a flow

chamber (thickness ~270 µm) under low tension (14). To remove glycerol, ATP, and BDM, prepared fibers were washed five times with rigor buffer consisting of (in mM) 120 K acetate, 5 Mg acetate, 5 EGTA, 2.5 K_2HPO_4, 2.5 KH_2PO_4, 50 MOPS, and 2 fresh DTT at pH 6.8 prior to imaging. Then the muscle bundles were incubated in rigor buffer containing 250µM mant-ATP (Sigma-Aldrich, Product # 18723), a fluorescent analogue of ATP for 5 min. All images were taken at 20x objective power under DAPI filter (excitation 360nm, emission 460nm) with a Hamamatsu 1394 ORCA-ERA camera equipped on a Leica DMi8 Widefield Fluorescence microscope every 4 seconds. After initial 60 seconds of background imaging, cardiac muscle preparations were washed with rigor buffer containing 4mM ATP to flush mant-ATP, and images were captured continually during this process for 6 min. We used a previously described biphasic pulse-chase protocol to measure single myosin nucleotide (ATP) turnover. First, rapid decay (~10 s) is a period of exchanging fluorescent nucleotides (mant-ATP) for ATP in disordered myosin heads, but unbound mant-ATP is also washed out of the fiber during this period (15). The subsequent slow phase of fluorescence decay shows lower rate of nucleotide exchange, because myosin heads are in highly ordered SRX state with reduced energy consumption. To measure fluorescence intensity, four different regions of interest (15µm x 20µm), three for fiber intensity and one for background intensity were selected. After subtracting background intensity from the averaged fiber fluorescence intensity, the value from each time point was normalized to the intensity of baseline value prior to mant-ATP washout. Fluorescence intensity results were fit to a double exponential decay

$$I = 1 - P_1\left(1 - e^{\frac{-t}{T1}}\right) - P_2\left(1 - e^{\frac{-t}{T2}}\right)$$

where I is the fluorescence intensity at any given time, *t*. The fast phase is described by the first exponent, and the second exponent describes the slow phase. P_x defines the relative proportions of fluorescence in each phase, and Tx is the lifetime (time constant) of that exponent, which is the inverse of the rate of ATP turnover. The percent approximation for myosin heads occupying the DRX state was calculated using 0.48 as the correction factor the percent approximation for myosin heads occupying the SRX state was then calculated as 100 - DRX (16).

Statistical analysis

For this study, all data were reported as mean ± S.E. The specific statistical tests for each assessed parameter can be found in the legends of figures and tables. $p < 0.05$ was considered statistically significant. SigmaPlot version 12 was used for data fitting and statistical analysis.

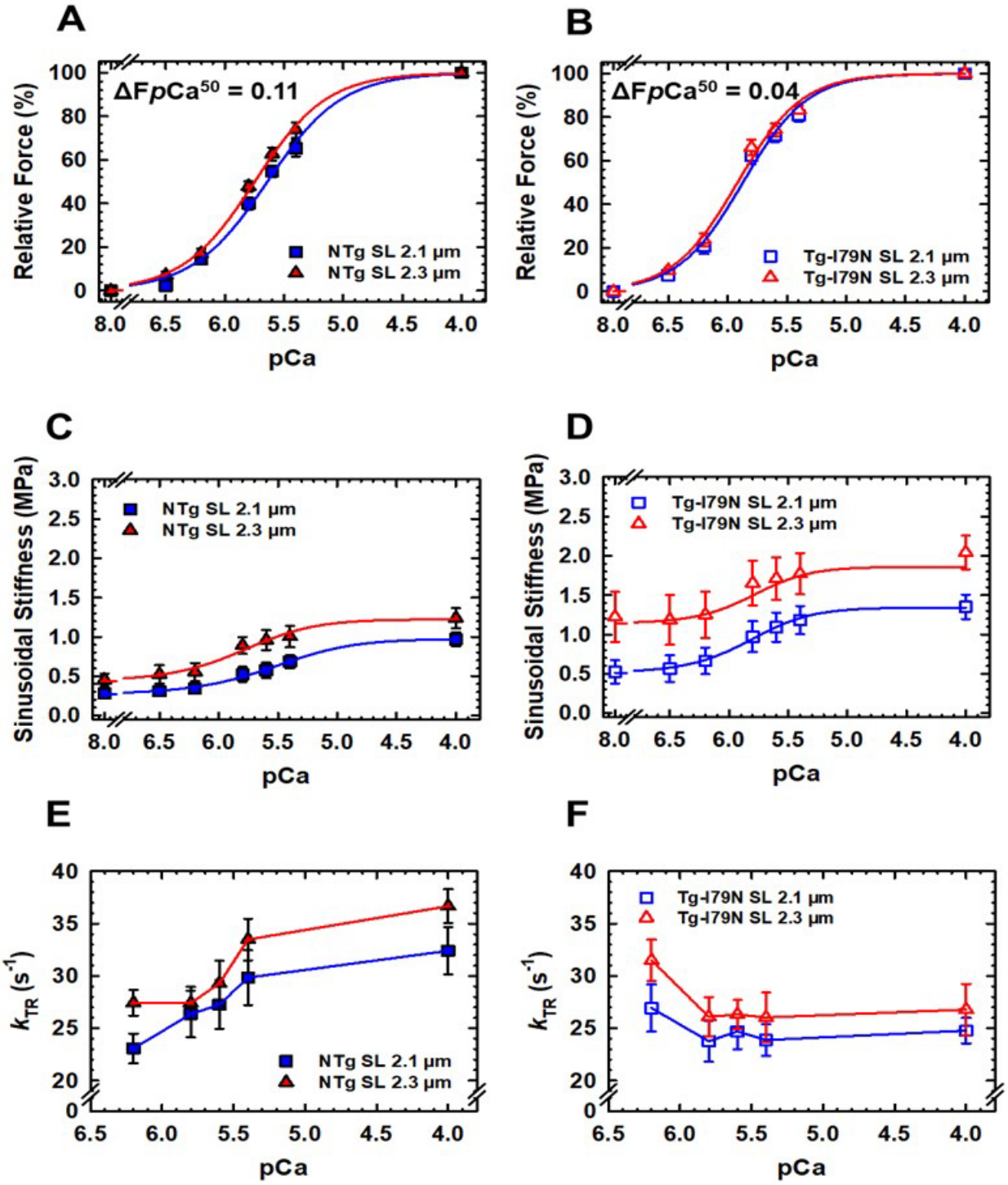

Supplementary figure 1. Effects of the cTnT-I79N variant on myofilament Ca^{2+} sensitivity (A-B), Ca^{2+}-dependence of (C-D) steady-state sinusoidal stiffness and (E-F) kinetics of tension redevelopment (k_{TR}). Data are shown as AVG ± S.E. (NTg, n= 6-8; Tg-I79N, n=7-8).

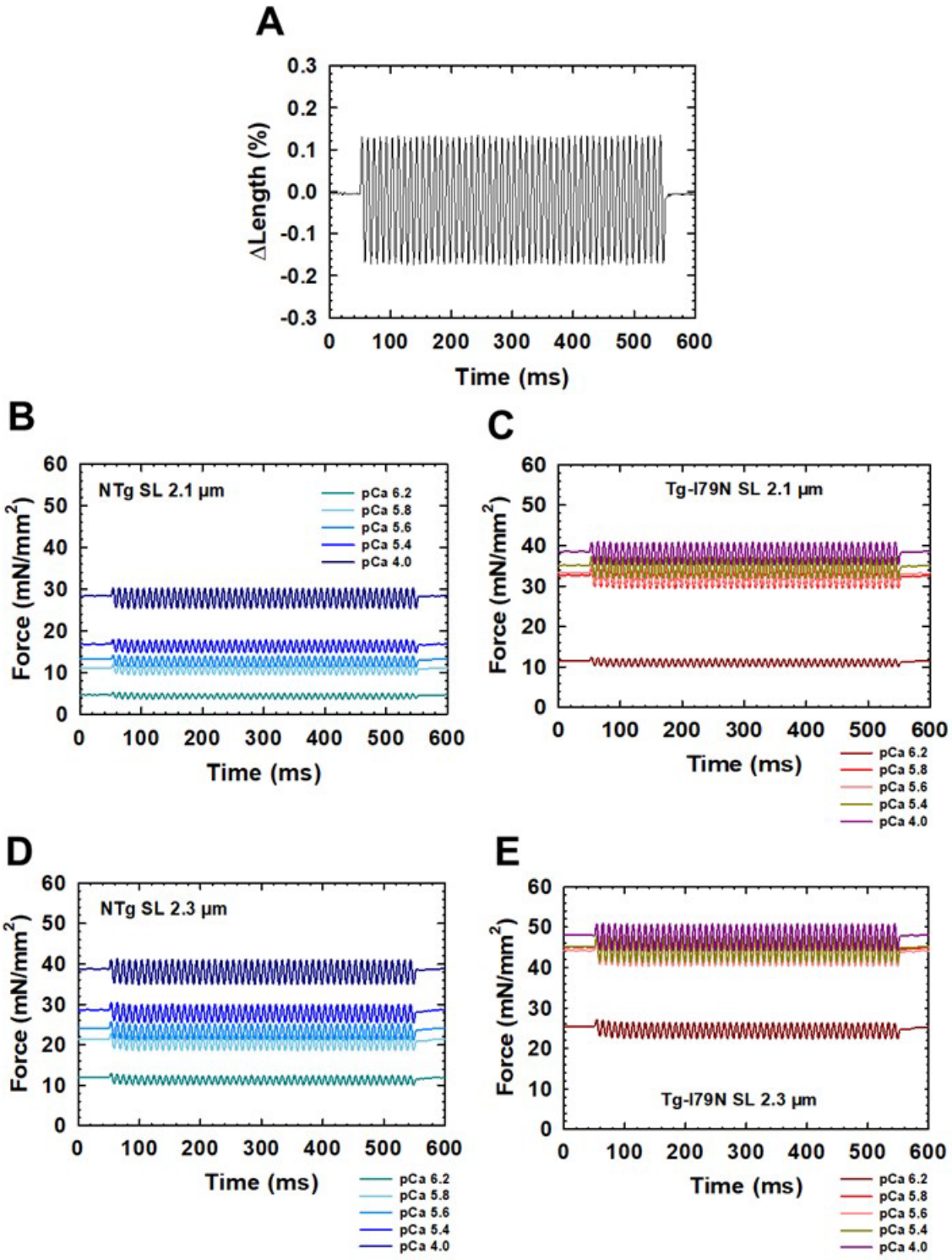

Supplementary figure 2. Sinusoidal stiffness tracings at different sarcomere lengths (SL). A) Representative trace of percentage length changes as a function of time. Representative traces of absolute force values at SL 2.1µm **(B and C)** and 2.3µm **(D and E)** as a function of time. The force values were normalized by the cross-sectional area of the cardiac muscle preparation.

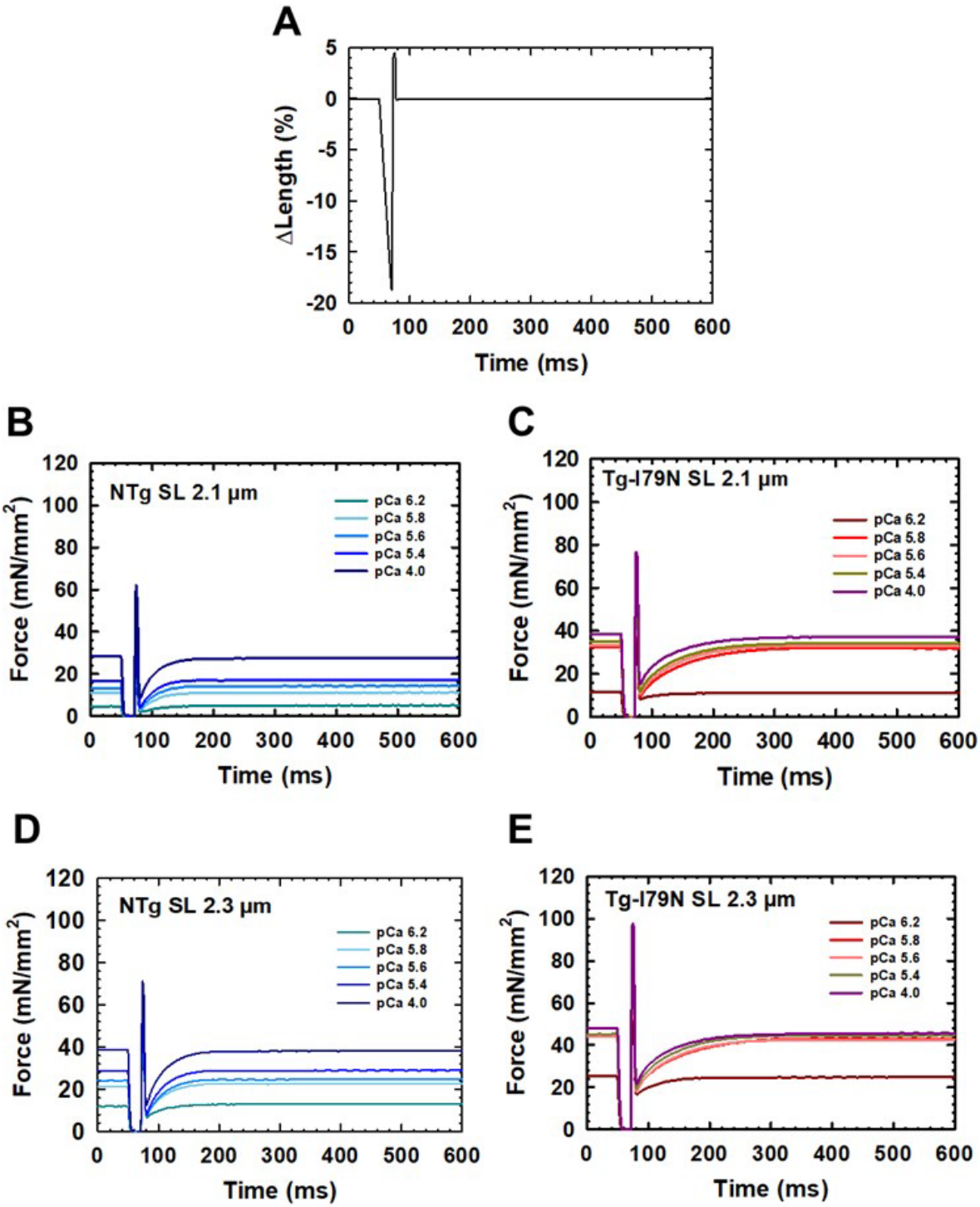

Supplementary figure 3. Kinetics of tension redevelopment tracings at different sarcomere lengths (SL). **A)** Representative trace of percentage length changes as a function of time. Representative traces of absolute force values at SL 2.1µm **(B and C)** and 2.3µm **(D and E)** as a function of time. The force values were normalized by the cross-sectional area of the cardiac muscle preparation.

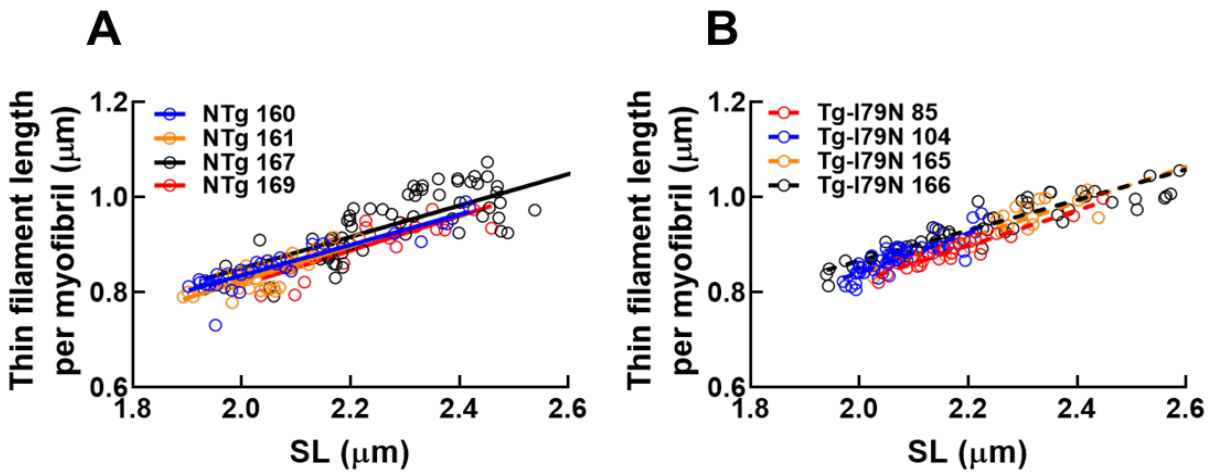

Supplementary figure 4. Effects of the cTnT-I79N variant on the cardiac thin filament length. A-B) Measurements of cardiac thin filament length per myofibril. Data are shown as individual points; NTg, n=4 animals; Tg-I79N, n=4 animals.

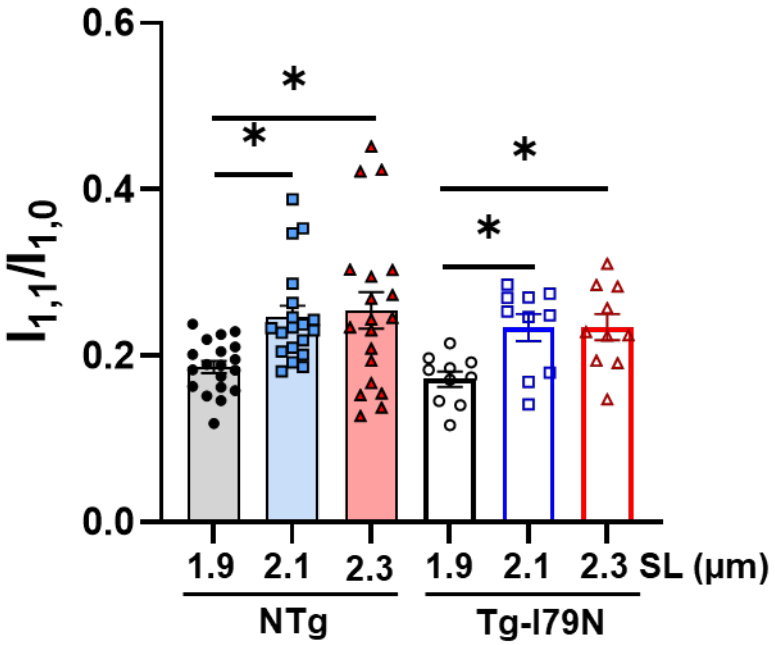

Supplementary Figure 5. Effects of the cTnT-I79N variant on Intensity ratio of the equatorial reflections $I_{1.1}$ and $I_{1.0}$ upon sarcomere length variation. Data are shown as AVG ± S.E.; NTg, n=19; Tg-I79N, n=10; statistical significance was assessed by One-way ANOVA with Tukey's post-hoc analysis; * $P < 0.05$ within the same genotype.

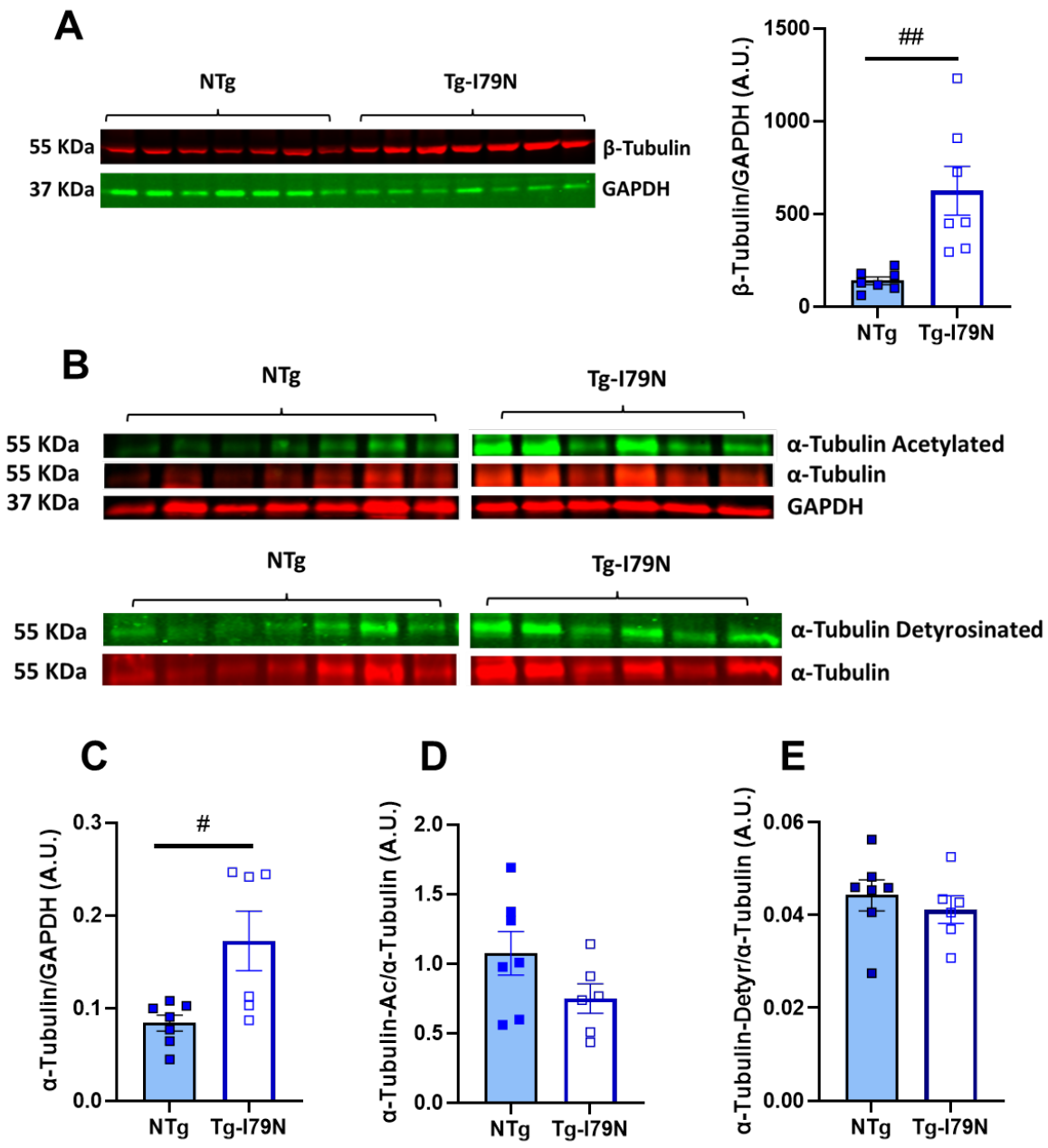

Supplementary Figure 6. Effects of the cTnT-I79N variant on PTMs of cardiac microtubule network. A) Cropped images of western immunoblotting membrane incubated with anti-GAPDH and -β-tubulin antibodies, and immunoblot quantification of β-tubulin. **B)** Cropped images of western immunoblotting membranes incubated with anti-GAPDH, -α-tubulin, -α-tubulin acetylated, and -α-tubulin detyrosinated antibodies. Immunoblot quantification of **C)** α-tubulin, **D)** α-tubulin acetylated, and **E)** α-tubulin detyrosinated. Tissue lysates from Tg-I79N and NTg left ventricles were used for the data collection showed in Figure 6. Data are shown as AVG ± S.E.; NTg, n=7; Tg-I79N, n=6; statistical significance was assessed by unpaired t-test analysis; # $P < 0.05$ between the genotypes.

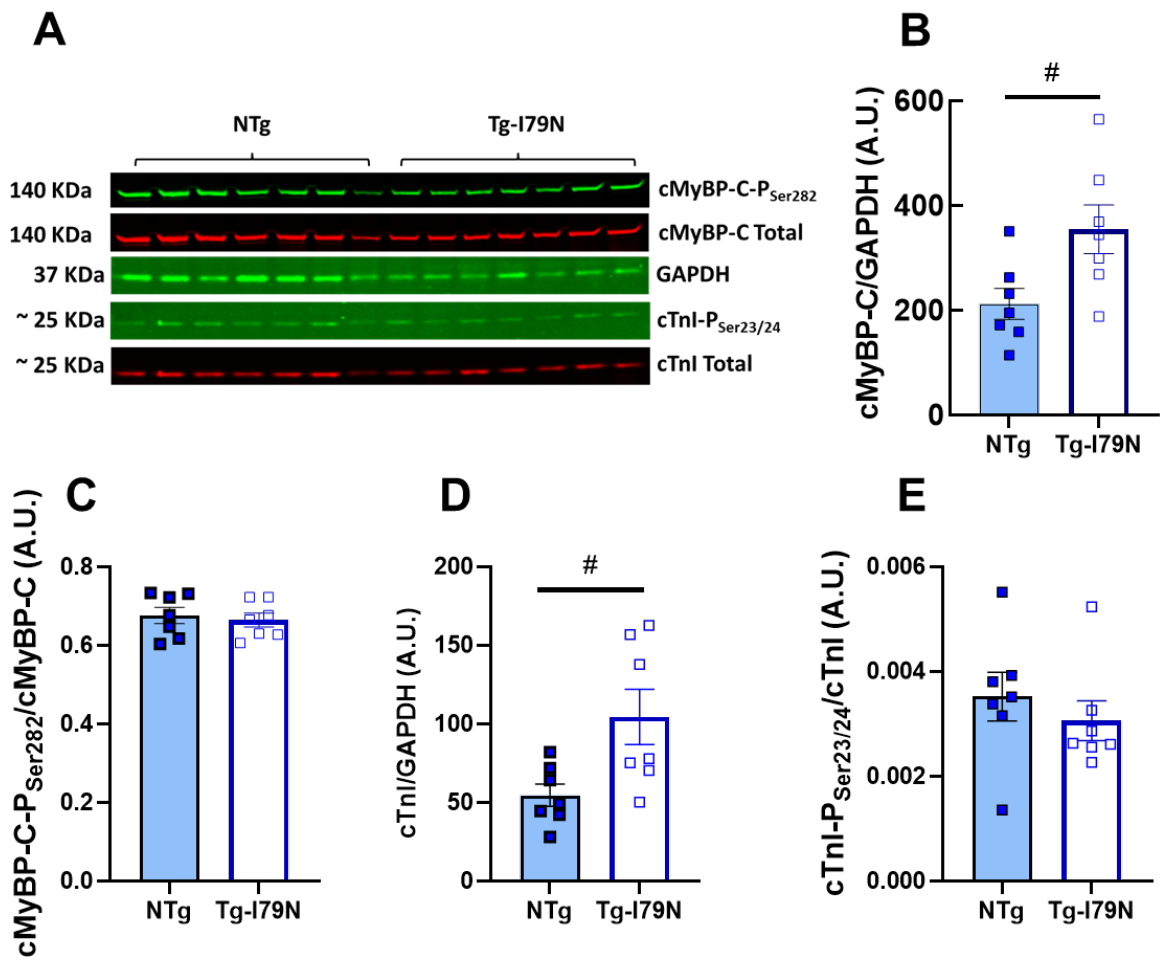

Supplementary Figure 7. Effects of the cTnT-I79N variant on PTMs of sarcomeric proteins. A) Cropped images of western immunoblotting membrane incubated with anti-cMyBP-C, -cMyBP-C-P$_{ser282}$, -GAPDH, -cTnI, and -cTnI-P$_{ser23/24}$ antibodies. Immunoblot quantification of **B)** cMyBP-C, **C)** cMyBP-C-P$_{ser282}$ normalized to cMyBP-C, **D)** cTnI, and **E)** cTnI-P$_{ser23/24}$ normalized by cTnI**.** Tissue lysates from Tg-I79N and NTg left ventricles were used for the data collection showed in Figure 7. Data are shown as AVG ± S.E.; NTg, n=7; Tg-I79N, n=7; statistical significance was assessed by unpaired t-test analysis; # $P < 0.05$ between the genotypes.

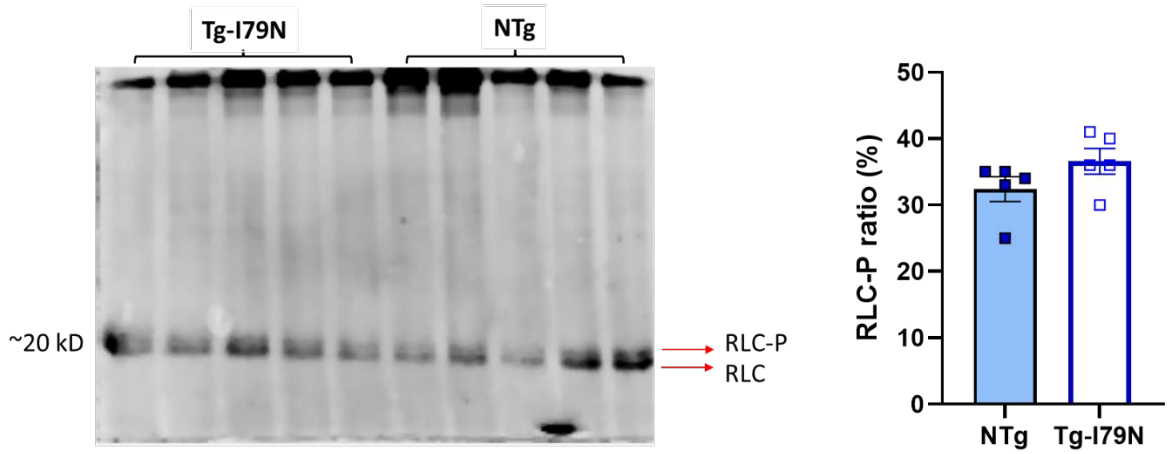

Supplementary Figure 8. Effects of the cTnT-I79N variant on myosin regulatory light chain (RLC) phosphorylation. Tissue lysates from Tg-I79N and NTg left ventricles were used for phos-tag gel followed by immunoblotting. RLC phosphorylation (RLC-P) ratio was quantified by dividing the intensity of the RLC-P (top band) over the sum of both non-phosphorylated plus phosphorylated intensities. Data are shown as AVG ± S.E.; NTg, n=5; Tg-I79N, n=5; statistical significance was assessed by unpaired t-test analysis.

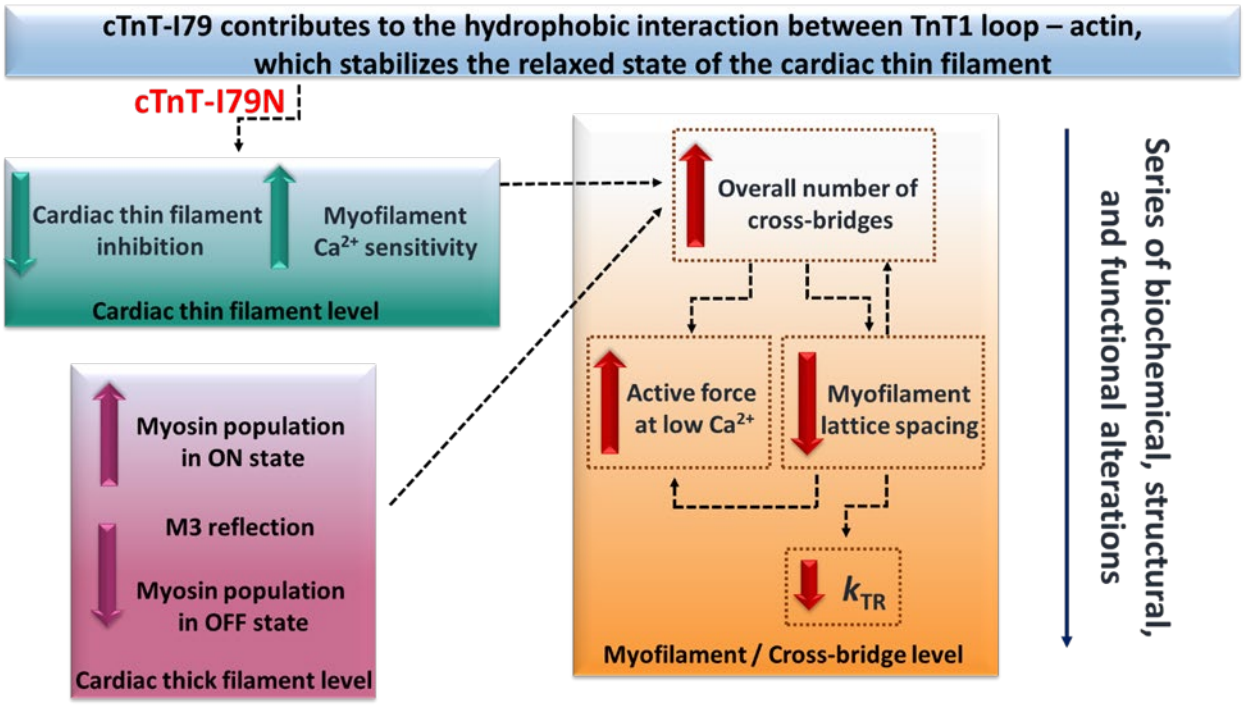

Supplementary Figure 9. Summary of biophysical, biochemical, and functional alterations caused by the cTnT-I79N variant.

Supplementary table 1. Contractile parameters measured in mouse permeabilized left ventricular papillary muscle as depicted in Figures 1 and 2.

	NTg		Tg-I79N	
	SL 2.1 µm	**SL 2.3 µm**	**SL 2.1 µm**	**SL 2.3 µm**
$F_{max\ (mN/mm^2)}$	17.80 ± 03.72	21.39 ± 04.38*	22.30 ± 02.48	24.60 ± 02.58*
$F_{pass\ (mN/mm^2)}$	00.79 ± 00.08	01.12 ± 00.16*	01.43 ± 00.36#	02.26 ± 00.49**, ##
F*p*Ca$_{50}$	05.63 ± 00.03	05.74 ± 00.03***	05.87 ± 00.05###	05.92 ± 00.04##
Fn_{Hill}	01.41 ± 00.08	01.48 ± 00.14	01.69 ± 00.14	01.67 ± 00.10
$k_{TR\ max}$ (s^{-1})	32.41 ± 02.27	36.67 ± 01.61	24.77 ± 01.22###	26.78 ± 02.46###
SS_{pass} (MPa)	00.26 ± 00.05	00.51 ± 00.17*	00.69 ± 00.19 #	01.47 ± 00.40*, #
SS_{max} (MPa)	00.97 ± 00.09	01.24 ± 00.13**	01.36 ± 00.15 ##	02.04 ± 00.21***, ##
#CMP	7 - 8	7 - 8	8	8

F_{max}, maximum steady-state isometric force; F_{pass}, passive steady-state isometric force values obtained at pCa 8 (resting condition); *p*Ca^{50}, Ca^{2+} concentration needed to reach 50% of the steady-state maximum force; n_{Hill}, cooperativity of thin filament activation; $k_{TR\ max}$, maximum rate of tension redevelopment; SS_{pass}, passive steady-state sinusoidal stiffness values obtained at pCa 8 (resting condition); SS_{max}, maximum steady-state sinusoidal stiffness; CMPs, cardiac muscle preparations. Data are shown as AVG ± S.E. (NTg, n= 7-8; Tg-I79N, n=8). Statistical significance was assessed by One-way ANOVA with Tukey's post-hoc analysis; *P < 0.05, **P < 0.01, *** P < 0.001 within the same genotype, and #P < 0.05, ##P < 0.01, ### P < 0.01 between genotypes.

	NTg	Tg-I79N
A-band width (µm)	01.61 ± 00.01	01.47 ± 00.02$^{\#\#\#}$
I-band width (µm)	00.37 ± 00.01	00.35 ± 00.01$^{\#}$
Z-line width (µm)	00.10 ± 00.01	00.10 ± 00.01
Sarcomere length (µm)	01.97 ± 00.01	01.78 ± 00.02$^{\#\#\#}$
#Sarcomeres	150 - 193	144 - 175
#animals	3	3

Supplementary table 2. Summary of the sarcomere ultrastructure's measurements obtained from longitudinal sections of left ventricular papillary muscle obtained from NTg and TG-I79N mice. Data are shown as AVG ± S.E.; NTg, n= 150-193; Tg-I79N, n= 144-175. Statistical significance was assessed by One-way ANOVA with Tukey's post-hoc analysis; #P < 0.05, ###P < 0.001 between the genotypes.

	NTg		Tg-I79N	
	SL 2.1µm	**SL 2.3µm**	**SL 2.1µm**	**SL 2.3µm**
Lattice Spacing (nm)	41.38 ± 00.17	40.27 ± 00.19***	40.72 ± 00.22#	39.12 ± 00.37***, ###
$I_{1,1}/I_{1,0}$	00.24 ± 00.01	00.25 ± 00.02	00.23 ± 00.01	00.23 ± 00.01
I_{M3}	00.78 ± 00.13	00.76 ± 00.11	00.51 ± 00.05###	00.44 ± 00.04###
#CMPs	13 - 19	13 - 19	9 - 10	9 - 10

Supplementary table 3. Summary of equatorial and meridional X-ray reflections. $I_{1.1}/I_{1.0}$ ratio, intensity ratio of the equatorial reflections $I_{1.1}$ and $I_{1.0}$; I_{M3}, Intensity of the meridional M3 reflection; CMPs, cardiac muscle preparations. Data are shown as AVG ± S.E.; NTg, n=19; Tg-I79N, n=10; statistical significance was assessed by One-way ANOVA with Tukey's post-hoc analysis; *** P < 0.001 within the same genotype, and #P < 0.05, ### P < 0.01 between genotypes.

	NTg		Tg-I79N	
	SL 2.1µm	**SL 2.3µm**	**SL 2.1µm**	**SL 2.3µm**
1,0 angle σ (rad)	00.19 ± 00.01	00.16 ± 00.01*****	00.20 ± 00.01	00.16 ± 00.01*******
1,0 width σ (10^{-3} nm^{-1})	07.07 ± 00.17	07.43 ± 00.31	07.04 ± 00.37	07.78 ± 00.36*****
#CMPs	25	23	10	10

Supplementary table 4. Summary of the angular standard deviation, and standard deviation of the 1,0 equatorial X-ray reflections in radial direction. Data are shown as AVG ± S.E.; NTg, n=23-25; Tg-I79N, n=10; statistical significance was assessed by One-way ANOVA with Tukey's post-hoc analysis; *P < 0.05, *** P < 0.001 within the same genotype.

	NTg SL 2.1 µm	Tg-I79N SL 2.1 µm
P1 (%)	00.72 ± 00.28	00.84 ± 00.03##
P2 (%)	00.23 ± 00.06	00.12 ± 00.01##
DRX (%)	34.51 ± 01.19	40.33 ± 00.77##
SRX (%)	65.49 ± 01.19	59.66 ± 00.77##
#CMPs	7	6

Supplementary table 5. Summary of mant-ATP fluorescence decay fast phase (P1) and slow phase (P2), and proportion of myosin heads in the DRX (disordered-relaxed state), and in the SRX (super-relaxed state). Data are shown as AVG ± S.E. (NTg, n=7; Tg-I79N, n=6). Statistical significance was assessed by One-way ANOVA with Tukey's post-hoc analysis; ## $P < 0.01$ between genotypes.

SI References

1. D. Dweck, A. Reyes-Alfonso, Jr., J. D. Potter, Expanding the range of free calcium regulation in biological solutions. *Anal Biochem* **347**, 303-315 (2005).
2. D. Gonzalez-Martinez *et al.*, Structural and functional impact of troponin C-mediated Ca(2+) sensitization on myofilament lattice spacing and cross-bridge mechanics in mouse cardiac muscle. *J Mol Cell Cardiol* **123**, 26-37 (2018).
3. M. A. Marques *et al.*, Anomalous structural dynamics of minimally frustrated residues in cardiac troponin C triggers hypertrophic cardiomyopathy. *Chem Sci* **12**, 7308-7323 (2021).
4. P. B. Chase, M. J. Kushmerick, Effects of pH on contraction of rabbit fast and slow skeletal muscle fibers. *Biophys J* **53**, 935-946 (1988).
5. T. Veltri *et al.*, Hypertrophic Cardiomyopathy Cardiac Troponin C Mutations Differentially Affect Slow Skeletal and Cardiac Muscle Regulation. *Front Physiol* **8**, 221 (2017).
6. J. R. Pinto *et al.*, Strong cross-bridges potentiate the Ca(2+) affinity changes produced by hypertrophic cardiomyopathy cardiac troponin C mutants in myofilaments: a fast kinetic approach. *J Biol Chem* **286**, 1005-1013 (2011).
7. J. M. de Winter *et al.*, KBTBD13 is an actin-binding protein that modulates muscle kinetics. *J Clin Invest* **130**, 754-767 (2020).
8. R. Fischetti *et al.*, The BioCAT undulator beamline 18ID: a facility for biological non-crystalline diffraction and X-ray absorption spectroscopy at the Advanced Photon Source. *J Synchrotron Radiat* **11**, 399-405 (2004).
9. J. Jiratrakanvong, Shao, J., Menendez, M., Li, X., Li, J., Ma, W., Agam, G. and, T. Irving, Musclex: software suite for diffraction x-ray imaging v1. 13.1. (2018).
10. W. Ma, H. Gong, T. Irving, Myosin Head Configurations in Resting and Contracting Murine Skeletal Muscle. *Int J Mol Sci* **19** (2018).
11. W. Ma *et al.*, Myofibril orientation as a metric for characterizing heart disease. *Biophys J* **121**, 565-574 (2022).
12. J. Jiratrakanvong *et al.*, MuscleX: software suite for diffraction X-ray imaging V1.13.1. doi:10.5281/zenodo.1195050. doi:10.5281/zenodo.1195050 (2018).
13. J. W. McNamara *et al.*, MYBPC3 mutations are associated with a reduced super-relaxed state in patients with hypertrophic cardiomyopathy. *PLoS One* **12**, e0180064 (2017).
14. J. W. McNamara *et al.*, Ablation of cardiac myosin binding protein-C disrupts the super-relaxed state of myosin in murine cardiomyocytes. *J Mol Cell Cardiol* **94**, 65-71 (2016).
15. R. Cooke, E. Pate, The effects of ADP and phosphate on the contraction of muscle fibers. *Biophys J* **48**, 789-798 (1985).
16. P. Hooijman, M. A. Stewart, R. Cooke, A new state of cardiac myosin with very slow ATP turnover: a potential cardioprotective mechanism in the heart. *Biophys J* **100**, 1969-1976 (2011).